Electronic Supplementary Material (ESI) for Physical Chemistry Chemical Physics.

Computational and Experimental Studies of the Wide Bandgap Semiconductors NH_4TiOF_3 and $(NH_4)_2TiOF_4$

Bingyu Lei,[a] Lisette Warren,[a] Carole Morrison,[a] Gwilherm Kerherve,[b] William S. J. Skinner,[b] David J. Payne,[c] and Neil Robertson*[a]

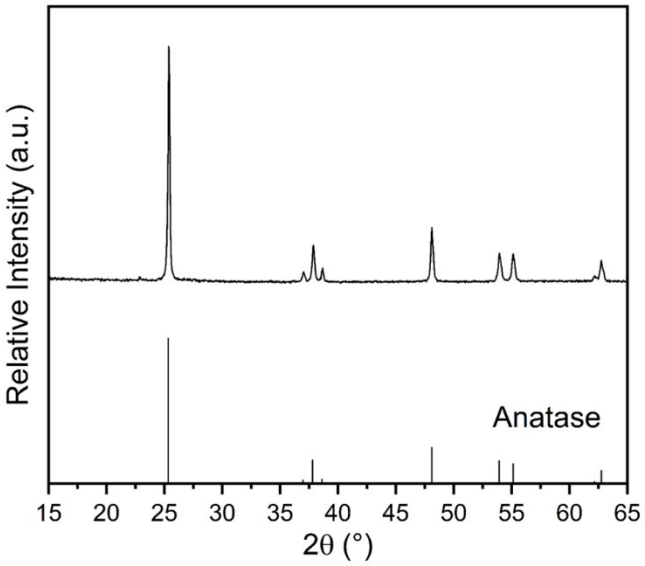

Figure S1 XRD pattern of the sample prepared by sintering NH_4TiOF_3 at 800 °C for 15 min, compared with standard PDF card (ICDD 86-1156) for anatase.

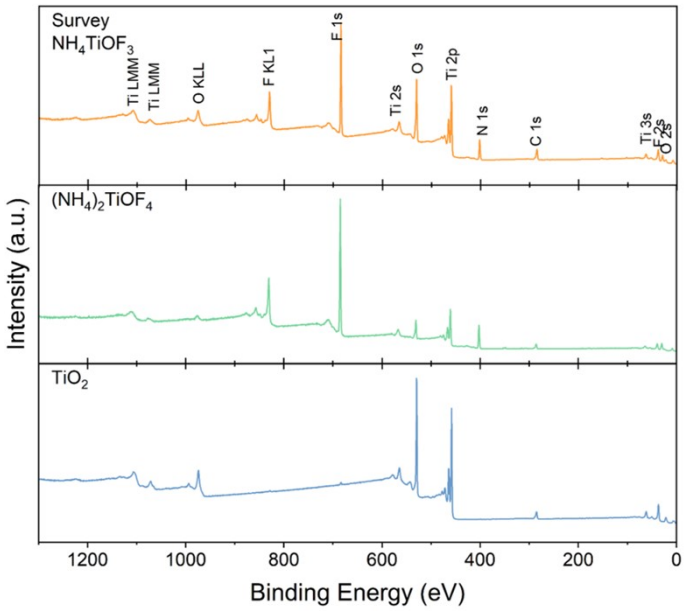

Figure S2 XPS survey spectra of (a) NH_4TiOF_3, (b) $(NH_4)_2TiOF_4$ and (c) TiO_2.

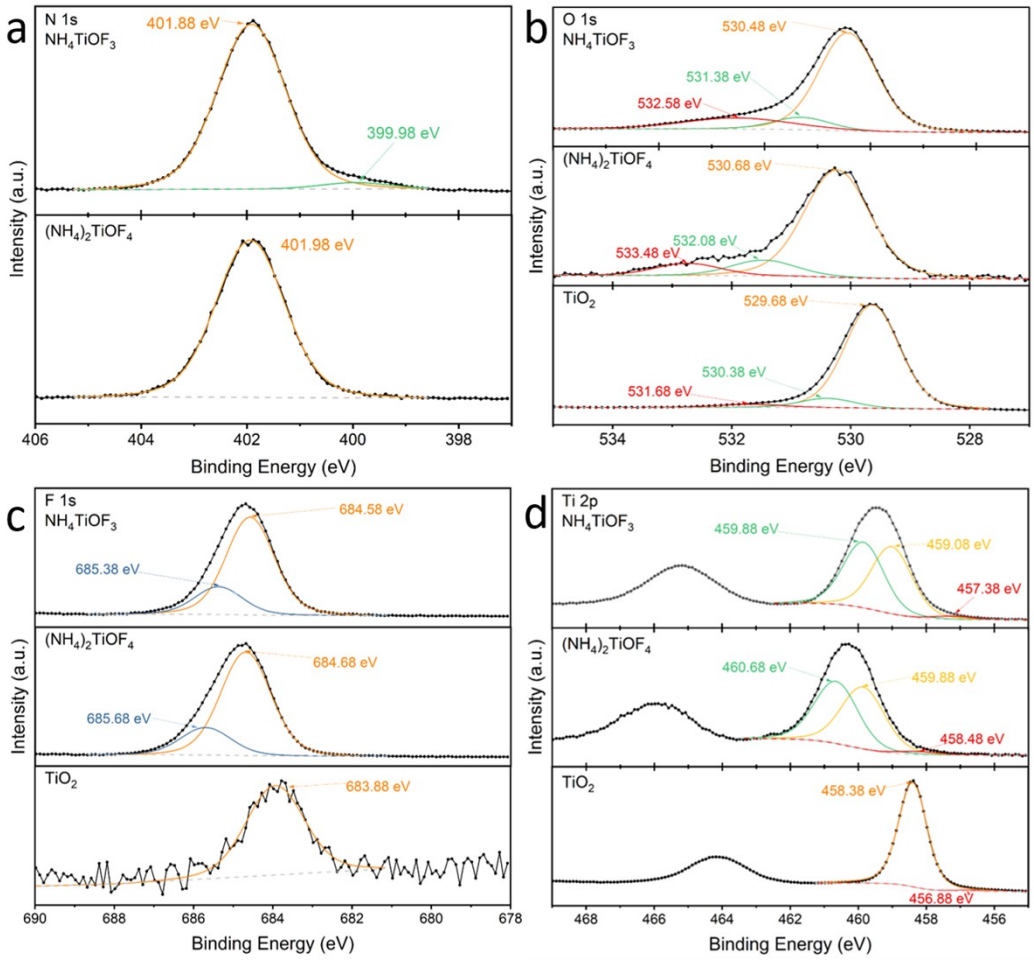

Figure S3 High-resolution XPS spectra of (a) N 1s (b) O 1s (c) F 1s and (d) Ti 2p.

Table S1 Bond lengths of NH_4TiOF_3 in the experimental data (labelled as single-point calculation) and after the geometry optimisation. Variation (Δ) was calculated referring to the experimental data.

Bond	Single-Point Calculation	Geometry Optimisation	Δ(%)
Ti1-O5	1.976	2.196	11.1
	1.901	1.680	-11.6
Ti1-F2	1.801	1.831	1.67
Ti1-F3	1.928	1.977	2.54
	1.906	1.964	3.04
Ti1-F4	1.863	1.938	4.03

Table S2 Bond angle of NH_4TiOF_3 in the experimental data (labelled as single-point calculation) and after the geometry optimisation. Variation (Δ) was calculated referring to the experimental data.

Bond	Single-Point Calculation	Geometry Optimisation	Δ(%)
F2-Ti1-F4	170.2	165.4	-2.82
F3-Ti1-F3	179.3	166.8	-6.97
Ti1-F3-Ti1	163.1	153.8	-5.70
O5-Ti1-O5	171.7	175.1	1.98
Ti1-O5-Ti1	153.8	150.5	-2.15

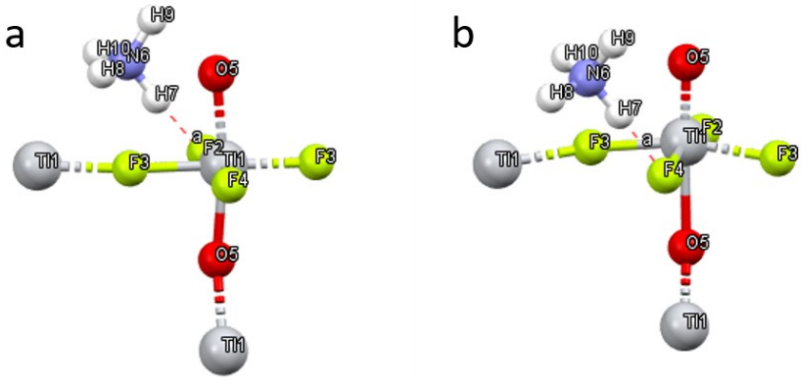

Figure S4 Structure of NH_4TiOF_3 (a) in the experimental data and (b) after the geometry optimisation.

The Ti-O distances changed from 1.976 and 1.901 to 2.196 and 1.680 after the geometry optimisation, which means the Ti atoms are more off-centred in the TiO_2F_4 octahedra in the ground state, or in other words, the O atoms are more unequally shared by two adjacent TiO_2F_4 octahedra. This led to the changes of the Ti-F distances and the variance of the bond angles F-Ti-F and O-Ti-O.

Table S3 Bond length of $(NH_4)_2TiOF_4$ in the experimental data (labelled as single-point calculation) and after the geometry optimisation. Variation (Δ) was calculated referring to the experimental data.

Bond	Single-Point Calculation	Geometry Optimisation	Δ(%)
Ti1-O2	1.95	1.91	-1.91
Ti1-F3	1.90	1.90	0.05
Ti1-F4	1.90	1.88	-0.61
Ti5-O6	1.95	1.89	-3.29
Ti5-F7	1.90	1.91	0.55
Ti5-F8	1.89	1.91	0.87

Table S4 Bond angle of $(NH_4)_2TiOF_4$ in the experimental data (labelled as single-point calculation) and after the geometry optimisation. Variation (Δ) was calculated referring to the experimental data.

Bond	Single-Point Calculation	Geometry Optimisation	Δ(%)
O2-Ti1-O2	180	180	0
F3-Ti1-F3	180	180	0
F4-Ti1-F4	180	180	0
Ti1-O2-Ti1	149.99	143.77	-4.15
O6-Ti5-O6	180	180	0
F7-Ti5-F7	180	180	0
F8-Ti5-F8	180	180	0
Ti5-O6-Ti5	150.58	149.75	-0.55

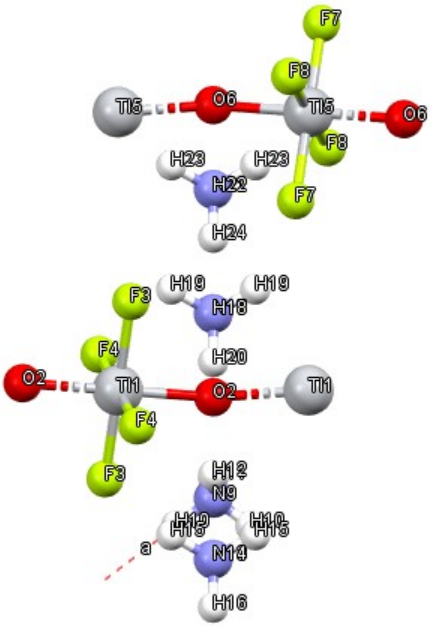

Figure S5 Structure of $(NH_4)_2TiOF_4$ with label of atoms.

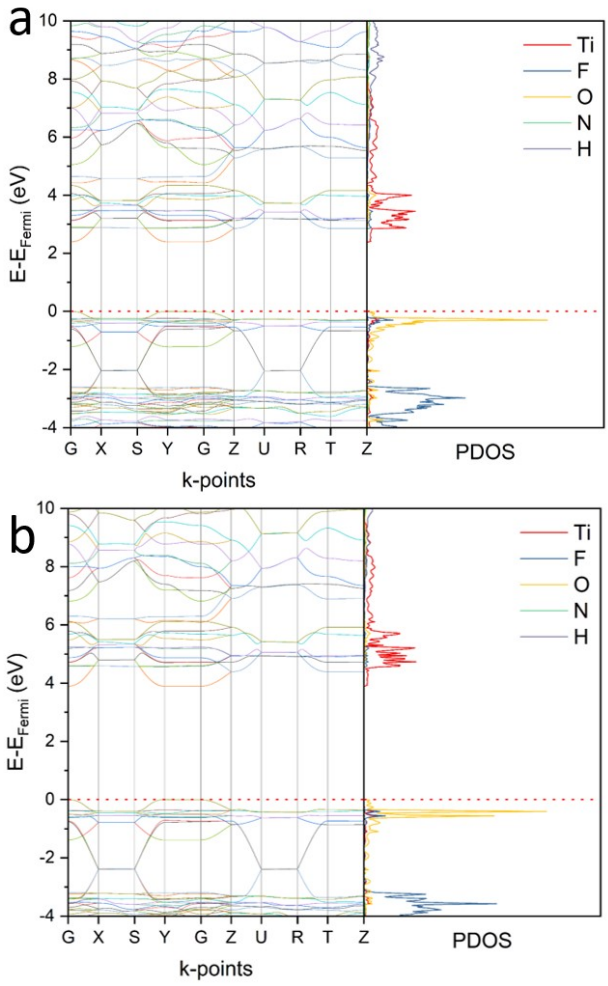

Figure S6 Computed band structures and corresponding PDOS of NH_4TiOF_3 using different functionals after the single-point energy calculation. (a) PBE-D3, E_{Fermi}= -5.35 eV, computed band gap: 2.39 eV; (b) B3LYP-D3, E_{Fermi}= -6.21 eV, computed band gap: 3.89 eV.

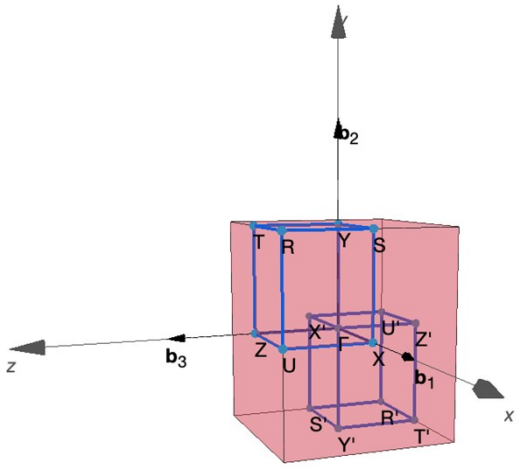

Figure S7 K-point path in the first Brillouin zone of NH_4TiOF_3.

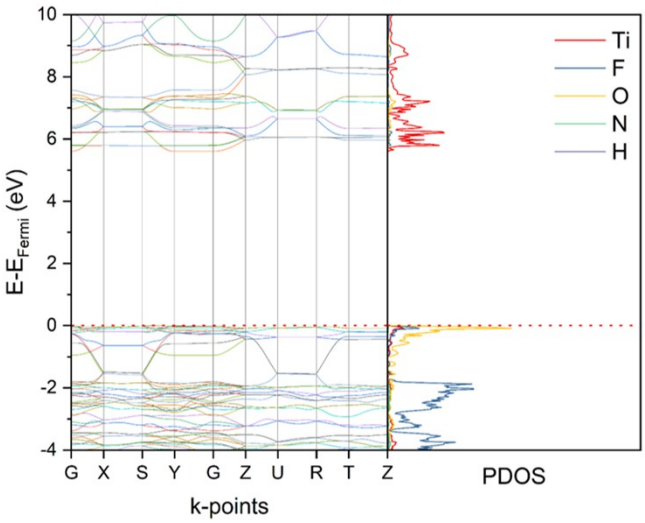

Figure S8 Computed density of states of NH_4TiOF_3 using HSE06-D3 after the geometry optimisation. E_{Fermi} = -7.75 eV.

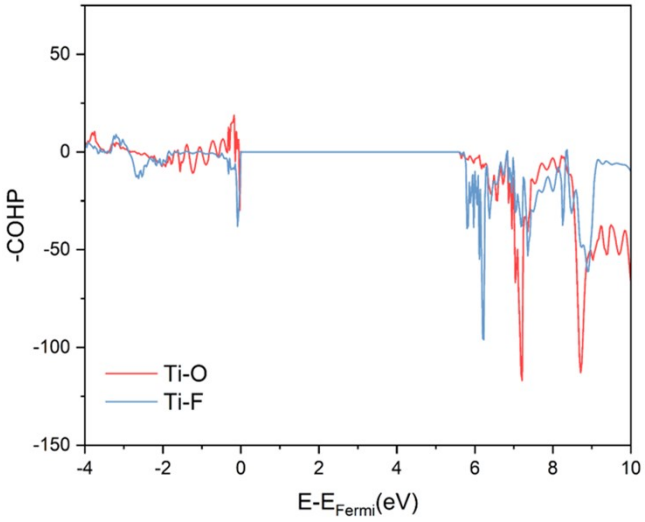

Figure S9 COHP of NH_4TiOF_3 over Ti-O (red line) and Ti-F (blue line) bonds, computed after geometry optimisation using HSE06-D3 functional.

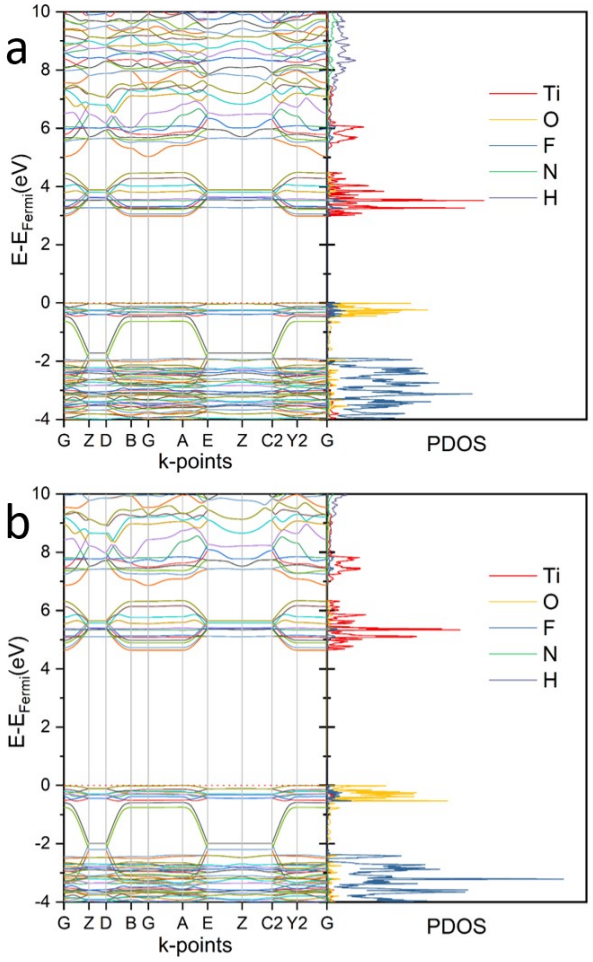

Figure S10 Computed band structures and corresponding PDOS of $(NH_4)_2TiOF_4$ using different functionals after the single-point energy calculation. (a) PBE-D3, E_{Fermi}= -5.52 eV, computed band gap: 2.98 eV; (b) B3LYP-D3, E_{Fermi}= - 6.50 eV, computed band gap: 4.64 eV.

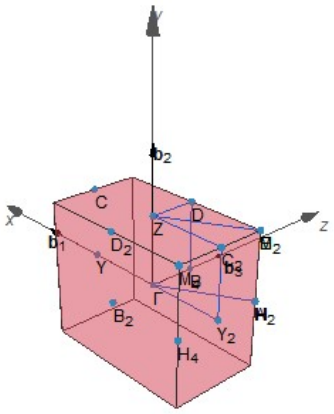

Figure S11 K-point path in the first Brillouin zone of $(NH_4)_2TiOF_4$.

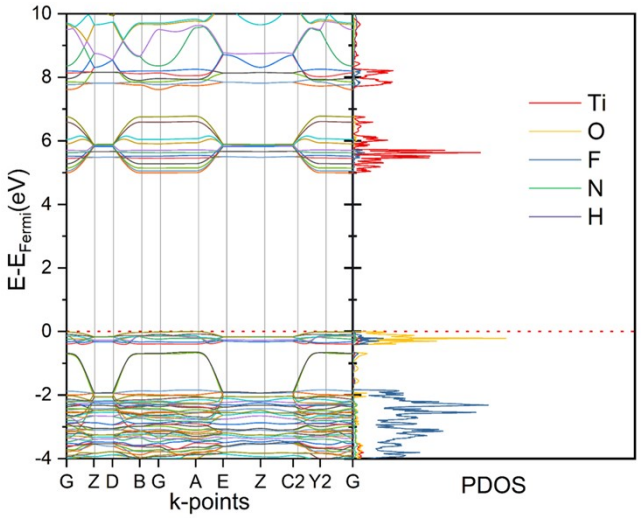

Figure S12 Computed band structure and density of states of $(NH_4)_2TiOF_4$ using HSE06-D3 after the geometry optimisation.

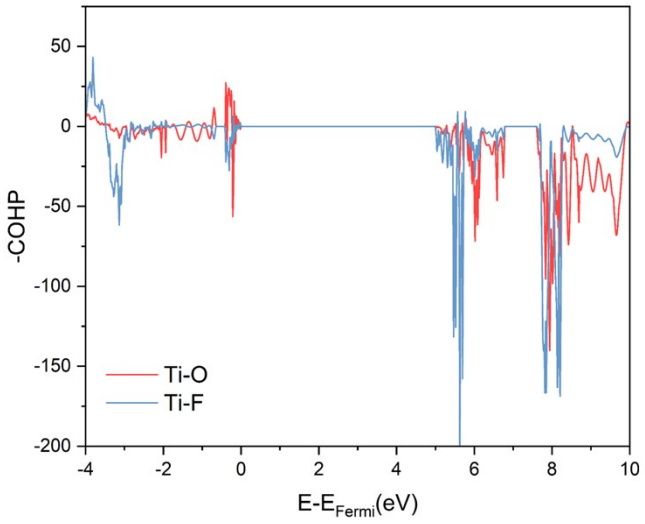

Figure S13 COHP of $(NH_4)_2TiOF_4$ over Ti-O (red line) and Ti-F (blue line) bonds, computed after geometry optimisation using HSE06-D3 functional.

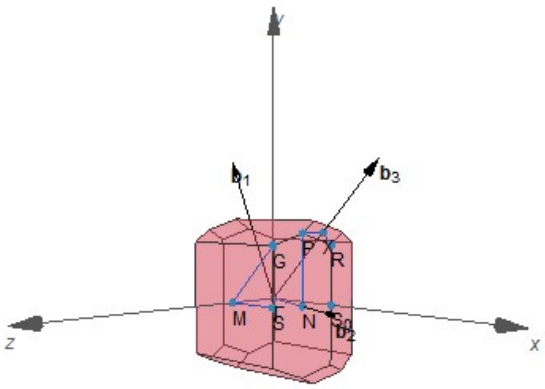

Figure S14 K-point path in the first Brillouin zone of anatase TiO_2.

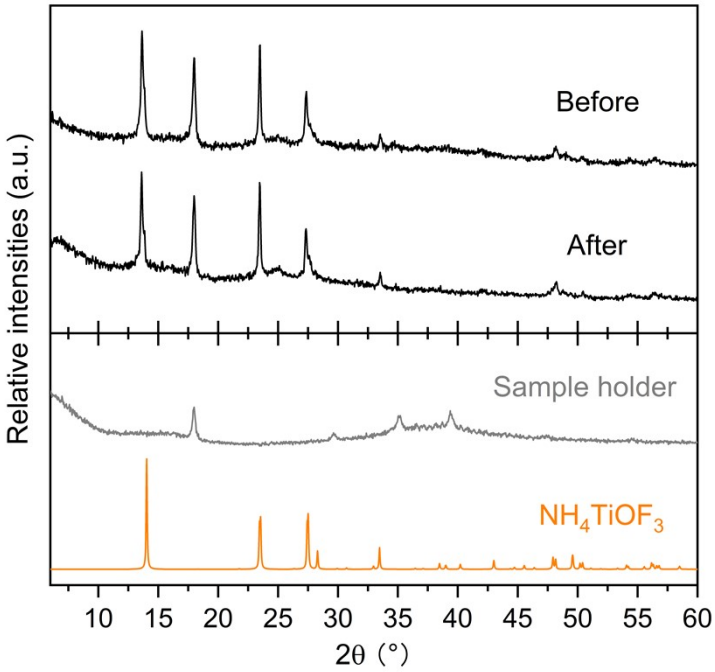

Figure S15 XRD patterns of the immobilised NH_4TiOF_3 sample before and after the photocatalysis test. A sample holder was used for the XRD measurements and the corresponding peaks are provided. NH_4TiOF_3: CCDC 1880514.

Table S5 Degradation rate constants of the immobilised NH_4TiOF_3, compared with immobilised P25 and no catalyst.

Sample	1st order rate constant (10^{-3} min^{-1})	
	RhB	MB
NH_4TiOF_3	9.26±0.02	9.28±0.98
P25	16.9±0.08	21.1±0.17
No catalyst	-0.48±0.01	0.23±0.04

Table S6 Adsorption efficiency of MB using different photocatalysts.

Sample	Adsorption efficiency of MB (%)
NH_4TiOF_3	24.3
P25	2.94
No catalyst	0.76

The adsorption efficiency was calculated by $(C_{MB} - C_0)/C_{MB}$, where C_{MB} is the initial concentration of the tested methylene blue solution and C_0 is the concentration at the light on point, i.e. after the dark adsorption.